

Research on Band Structure of One-dimensional Phononic Crystals Based on Wavelet Finite Element Method

Mao Liu^{1,2}, Jiawei Xiang¹, Haifeng Gao¹, Yongying Jiang¹, Yuqing Zhou¹
and Fengping Li¹

Abstract: A wavelet finite element method (WFEM) is developed to analyze the dispersion relation for one-dimensional phononic crystals (1DPCs). In order to calculate the band gaps (BGs) of 1DPCs, the wavelet finite element model is constructed using a slender beam element based on B-spline wavelet on the interval (BSWI). Combining with the Bloch-Floquet theorem and $\omega(k)$ technique, the model will be simplified as a simple eigenproblem. The performance of the proposed method has been numerically verified by one numerical example.

Keywords: Wavelet finite element, Band gaps, Phononic crystals, Dynamic characteristic, slender beam.

1 Introduction

Phononic crystals (PCs) are artificial materials with a periodic structure and were first investigated in the early seventies of the last century. The study of wave propagation in periodic structures has originated many novel discoveries in physics. Since the 1990s, there has been a great deal of work devoted to the study of phononic crystals [Kushwaha et al. (1993); Tarasenko et al. (2004)]. The existence of phononic BGs where the propagation of acoustic or elastic waves is forbidden exhibits a lot of potential applications, such as noise reduction, waveguides, acoustic filters, etc. Therefore, the mechanism for tuning the band gap is always an important topic of the theoretical studies of PCs.

One of the most major content of phononic crystals is its band structure calculations. There are several numerical methods to calculate band structures. The plan-wave expansion (PWE) [Kushwaha et al. (1994); Tanaka and Tamura (1999)]

¹ College of Mechanical & Electrical Engineering, Wenzhou University, Wenzhou, 325035, P.R. China.

² School of Mechanical and Electrical Engineering, Guilin University of Electronic Technology, Guilin, 541004, P.R. China.

is a powerful tool to investigate wave propagation problems and band structures. However, to deal with the problems of varied material parameters of components, the convergence is slow. Besides, when the classical PWE method is employed to solve fluid-solid PCs, the fictitious transversal modes are often occurred. Therefore, the extended PWE (EPWE) technique was presented to calculate fluid-solid PCs [Moiseyenko and Laude (2011)]. Moreover, the finite-difference time-domain method (FDTD) was developed to obtain the unique solutions of PCs with nonlinear material properties in a natural way [Tanaka and Tamura (1998)]. However, FDTD can not be applied to PCs structures with complex geometry. Finite element method (FEM) is suitable to solve structural mechanics problems in complicated domains and then introduced to calculate band gaps (BGs) of PCs [Assouar and Oudich (2011)]. FEM models of PCs lead to an eigenvalue problem, which is usually solved for the unknown frequencies (ω) with a real wave number (k), i.e., the $\omega(k)$ technique [Assouar and Oudich (2011)]. Recently, boundary element method is proposed to solve band gaps of PCs with good performance [Gao et al. (2013a, 2013b)].

Wavelet finite element method (WFEM) is developed in recent years as a new numerical method using scale function or/and wavelet function to replace the traditional polynomial as approximating function. Ko et al. constructed a class of one-dimensional wavelet based element by using orthogonal Daubechies wavelet [Ko et al. (1997)]; Chen et al. proposed wavelet-based elements using Daubechies wavelet, B-spline wavelet wavelet on the interval (BSWI) respectively to analysis structural problems and developed adaptive WFEM [Chen et al. (2004, 2010, 2012)]; Hang et al. extended the WFEM by using mixed variational principle [Hang et al. (2005, 2006)]; He and Ren continued to develop WFEM [He and Ren (2013a, 2013b)]. By utilizing multi-resolution characteristics, we can obtain a variety of wavelet-based elements to solve partial differential equations (PDEs) in engineering. Since BSWI scale functions at all level have the analytical expression, the elemental stiffness and mass matrices can be calculated conveniently [Xiang et al. (2007, 2008a, 2008b)]. Therefore, the wavelet finite element method has been successfully applied to solve stress intensity factor [Xiang et al. (2012)] and damage detection field [Xiang and Liang (2011), Xiang et al. (2011), Li and Dong (2012), Li and He (2013)]. Furthermore, for one-dimensional structures there have been applications of WFEM for curved beams [Yang et al. (2014)] and wave motion analysis in arch structures [Yang et al. (2014)]. For two-dimensional structures, the vibration analysis of curved shell [Yang et al. (2012)] and free vibration and buckling analysis of plates [Yang et al. (2013)] are investigated using WFEM. Recently, WFEM was summarized by Li and Chen and the classification and further research directions were given [Li and Chen (2014)]. Therefore, the WFEM is an effective

numerical simulation method in structure analysis.

In this paper, we employed the wavelet-based element to construct FEM model of one-dimensional phononic crystals (1DPCs). The numerical dispersion relation of 1DPCs will be presented and it will be shown that for rational wave vectors, a polynomial eigenvalue problem will be obtained. The BGs of 1DPCs are calculated using BSWI elements at different wavelet level. The results are verified and compared with the traditional finite element method.

2 WFEM model of 1DPCs

BGs for periodic structures are usually calculated in the frequency domain by utilizing unit cells and periodic boundary conditions (BCs). The same principle will be followed in the presented paper to investigate 1DPCs using wavelet-based element. Fig.1 shows the schematic structure of 1DPCs made of a series of identical segments. Each segment includes two differential materials for A and B (A and B have the same cross-section) with their thickness are a_1 and a_2 , respectively. The thickness (lattice constant or periodic distance) of a unit cell (lattice constant) is $a = a_1 + a_2$.

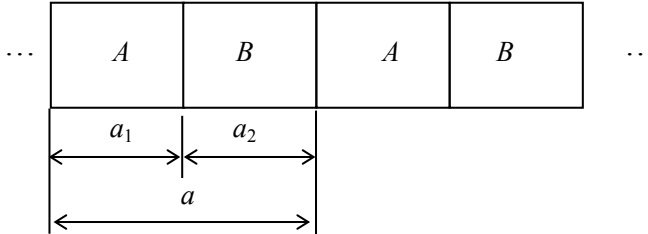


Figure 1: Schematic structure of 1DPCs.

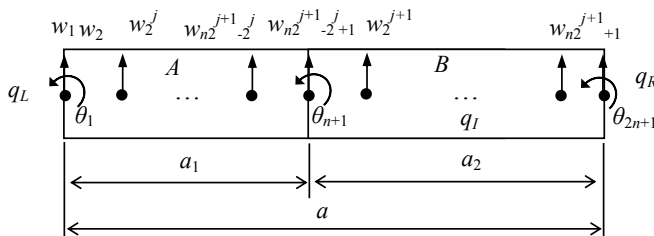


Figure 2: The diagram of a segment represented by $2n$ BSWI 4_j elements.

Fig.2 shows a unit cell of the structure. Consider the periodic characteristic, we can solve the band structure only using a unit cell of 1DPCs. Therefore, we focus on the calculation model using wavelet-based element on a unit cell. Suppose $2n$ BSWI 4_j (4 is the order of BSWI bases [Xiang et al, (2008a)], j is the wavelet level) Euler beam elements [Xiang et al. (2007)] (n elements supported on section A and the other n elements supported on section B) are employed to discretize the unit cell, the degrees of freedom (DOF) corresponding to the node on the left hand boundary q_L is $\mathbf{v}_L = \{w_1, \theta_1\}^T$, the node on the right hand boundary q_R is $\mathbf{v}_R = \{w_{n2^{j+1}+1}, \theta_{2n+1}\}^T$ and the other inner nodes is $\mathbf{v}_I = \{w_2, w_3, \dots, w_{2^j}, w_{2^{j+1}}, \theta_2, \dots, w_{n2^{j+1}-2^{j+1}}, \dots, w_{n2^{j+1}}, w_{n2^{j+1}+1}, \theta_{2n+1}\}^T$.

Thus, the total DOF of a unit cell is

$$\mathbf{v} = \begin{pmatrix} \mathbf{v}_L \\ \mathbf{v}_I \\ \mathbf{v}_R \end{pmatrix} \tag{1}$$

Corresponding to DOF in a unit cell, there will be a generalized force as [Veres and Berer, (2012)]

$$\mathbf{F} = \begin{pmatrix} \mathbf{F}_L \\ \mathbf{F}_I \\ \mathbf{F}_R \end{pmatrix} \tag{2}$$

where \mathbf{F}_L , \mathbf{F}_R and \mathbf{F}_I are the generalized force on the left hand boundary, the right hand boundary and the other inner nodes.

When a free wave propagates through an infinite structure, \mathbf{F}_I is zero. At this point, the periodic boundary conditions are not yet applied. Therefore, according to Bloch-Floquet theorem, the propagation constants between the nodes on left and right hand boundaries (exterior nodes) of a unit cell are given as e^{ika} (k is the wave number and i is the imaginary unit). The generalized forces at the exterior nodes, i.e., \mathbf{F}_L and \mathbf{F}_R , are not zero, since these forces are responsible for transmitting the wave motion.

Because \mathbf{v}_L and \mathbf{v}_R are separated by the periodic distance a , the relationship of the two DOF on the exterior nodes can be represented by [Veres and Berer (2012)]

$$\mathbf{v}_R = e^{ika} \mathbf{v}_L \tag{3}$$

Similarly, the corresponding \mathbf{F}_L and \mathbf{F}_R should have the relationship as

$$\mathbf{F}_R = -e^{ika} \mathbf{F}_L \tag{4}$$

Therefore, the equation of motion of a unit cell (periodic section) is [Veres and Berer (2012)]

$$(\mathbf{K}^j - \omega^2 \mathbf{M}^j) \begin{Bmatrix} \mathbf{v}_L \\ \mathbf{v}_I \\ \mathbf{v}_L e^{ika} \end{Bmatrix} = \begin{Bmatrix} \mathbf{F}_L \\ 0 \\ -\mathbf{F}_L e^{ika} \end{Bmatrix} \quad (5)$$

where ω is the angular frequency (rad/s), \mathbf{K}^j and \mathbf{M}^j are the global stiffness and mass matrices of a unit cell and the corresponding superscripts j are also the wavelet level.

Because a unit cell consist of $2n$ BSWI4 _{j} Euler beam elements, \mathbf{K}^j and \mathbf{M}^j are formed by superposition of $\mathbf{K}^{A,j}$ (the superposition of BSWI4 _{j} Euler beam element stiffness matrices $\mathbf{K}^{eA,j}$ of section A) and $\mathbf{K}^{B,j}$ (the superposition of BSWI4 _{j} Euler beam element stiffness matrices $\mathbf{K}^{eB,j}$ of section B), $\mathbf{M}^{A,j}$ (the superposition of BSWI4 _{j} Euler beam element mass matrices $\mathbf{M}^{eA,j}$ of section A) and $\mathbf{M}^{B,j}$ (the superposition of BSWI4 _{j} Euler beam element mass matrices $\mathbf{M}^{eB,j}$ of section B). The BSWI4 _{j} Euler beam element stiffness and mass matrices $\mathbf{K}^{eA,j}$, $\mathbf{K}^{eB,j}$, $\mathbf{M}^{eA,j}$ and $\mathbf{M}^{eB,j}$ are [Xiang et al. (2007)]

$$\mathbf{K}^{eA,j} = \frac{E_1 I}{(a_1/n)^3} \int_0^1 (\mathbf{T}_1^e)^T \left(\frac{d^2 \boldsymbol{\varphi}^T}{d\xi^2} \right) \left(\frac{d^2 \boldsymbol{\varphi}}{d\xi^2} \right) \mathbf{T}_1^e d\xi \quad (6)$$

$$\mathbf{K}^{eB,j} = \frac{E_2 I}{(a_2/n)^3} \int_0^1 (\mathbf{T}_2^e)^T \left(\frac{d^2 \boldsymbol{\varphi}^T}{d\xi^2} \right) \left(\frac{d^2 \boldsymbol{\varphi}}{d\xi^2} \right) \mathbf{T}_2^e d\xi \quad (7)$$

$$\mathbf{M}^{eA,j} = (a_1/n) \rho_1 S \int_0^1 (\mathbf{T}_1^e)^T \boldsymbol{\varphi}^T \boldsymbol{\varphi} \mathbf{T}_1^e d\xi \quad (8)$$

$$\mathbf{M}^{eB,j} = (a_2/n) \rho_2 S \int_0^1 (\mathbf{T}_2^e)^T \boldsymbol{\varphi}^T \boldsymbol{\varphi} \mathbf{T}_2^e d\xi \quad (9)$$

in which E_1 and E_2 , ρ_1 and ρ_2 are the Young's moduli and material densities of the two sections A and B, respectively, I and S are the moment of inertia, the area of cross-section for the two sections A and B, respectively, $\boldsymbol{\varphi}$, \mathbf{T}_1^e and \mathbf{T}_2^e are the column vector combined by the BSWI scaling functions for 4th order at the level j , the transformation matrices, respectively, as [Xiang et al. (2008a)]

$$\boldsymbol{\varphi} = \left\{ \varphi_{4,-3}^j(\xi), \varphi_{4,-2}^j(\xi), \dots, \varphi_{4,2j-1}^j(\xi) \right\} \quad (10)$$

$$\mathbf{T}_1^e = \left([\boldsymbol{\varphi}^T(\xi_1), \frac{1}{a_1/n} \frac{d\boldsymbol{\varphi}^T(\xi_1)}{d\xi}, \boldsymbol{\varphi}^T(\xi_2), \dots, \boldsymbol{\varphi}^T(\xi_r), \boldsymbol{\varphi}^T(\xi_{r+1}), \frac{1}{a_1/n} \frac{d\boldsymbol{\varphi}^T(\xi_{r+1})}{d\xi}]^T \right)^{-1} \tag{11}$$

$$\mathbf{T}_2^e = \left([\boldsymbol{\varphi}^T(\xi_1), \frac{1}{a_2/n} \frac{d\boldsymbol{\varphi}^T(\xi_1)}{d\xi}, \boldsymbol{\varphi}^T(\xi_2), \dots, \boldsymbol{\varphi}^T(\xi_r), \boldsymbol{\varphi}^T(\xi_{r+1}), \frac{1}{a_2/n} \frac{d\boldsymbol{\varphi}^T(\xi_{r+1})}{d\xi}]^T \right)^{-1} \tag{12}$$

in which $r = 2^j$ and the scaling functions $\varphi_{4,-3}^j(\xi), \varphi_{4,-2}^j(\xi), \dots, \varphi_{4,2^j-1}^j(\xi)$ are shown in. [Xiang et al. (2008a)].

To simple the calculation, the global stiffness and mass matrices are partitioned to nine sub-blocks in associated with the three types of nodes, i.e., a node on the left hand boundary, a node on the right hand boundary and nodes on the interior. Thus, we have

$$\mathbf{K}^j = \begin{bmatrix} \mathbf{K}_{LL} & \mathbf{K}_{LI} & \mathbf{K}_{LR} \\ \mathbf{K}_{IL} & \mathbf{K}_{II} & \mathbf{K}_{IR} \\ \mathbf{K}_{RL} & \mathbf{K}_{RI} & \mathbf{K}_{RR} \end{bmatrix} \tag{13}$$

and

$$\mathbf{M}^j = \begin{bmatrix} \mathbf{M}_{LL} & \mathbf{M}_{LI} & \mathbf{M}_{LR} \\ \mathbf{M}_{IL} & \mathbf{M}_{II} & \mathbf{M}_{IR} \\ \mathbf{M}_{RL} & \mathbf{M}_{RI} & \mathbf{M}_{RR} \end{bmatrix} \tag{14}$$

where $L = 2, I = n2^{j+1} + 2n - 2, R = 2$.

In the present, we only calculate the band structure of PCs. Therefore, the generalized force matrix becomes zero and the equation of free vibration is

$$(\mathbf{K}^j - \omega^2 \mathbf{M}^j) \begin{Bmatrix} \mathbf{v}_L \\ \mathbf{v}_I \\ \mathbf{v}_R \end{Bmatrix} = 0 \tag{15}$$

According to [Mead et al. (1973)], submitting Eq.(3) into Eq.(15), we have

$$\begin{bmatrix} \mathbf{K}_{LL} + \mathbf{K}_{RR} + e^{ika} \mathbf{K}_{LR} + e^{-ika} \mathbf{K}_{RL} & \mathbf{K}_{LI} + e^{-ika} \mathbf{K}_{RL} \\ \mathbf{K}_{IL} + e^{ika} \mathbf{K}_{IR} & \mathbf{K}_{II} \end{bmatrix} \begin{Bmatrix} \mathbf{v}_L \\ \mathbf{v}_I \end{Bmatrix} - \omega^2 \begin{bmatrix} \mathbf{M}_{LL} + \mathbf{M}_{RR} + e^{ika} \mathbf{M}_{LR} + e^{-ika} \mathbf{M}_{RL} & \mathbf{M}_{LI} + e^{-ika} \mathbf{M}_{RL} \\ \mathbf{M}_{IL} + e^{ika} \mathbf{M}_{IR} & \mathbf{M}_{II} \end{bmatrix} \begin{Bmatrix} \mathbf{v}_L \\ \mathbf{v}_I \end{Bmatrix} = 0 \tag{16}$$

By separating real and imaginary parts [Wilkinson (1965)] and let $\mathbf{K} = \mathbf{K}^r + i\mathbf{K}^i$ and $\mathbf{M} = \mathbf{M}^r + i\mathbf{M}^i$, Eq. (16) becomes

$$\left\{ \left[\begin{array}{cc} \mathbf{K}^r & \mathbf{K}^i \\ \mathbf{K}^i & \mathbf{K}^r \end{array} \right] - \omega^2 \left[\begin{array}{cc} \mathbf{M}^r & \mathbf{M}^i \\ \mathbf{M}^i & \mathbf{M}^r \end{array} \right] \right\} \left\{ \begin{array}{c} \mathbf{v}_L \\ \mathbf{v}_I \end{array} \right\} = 0 \quad (17)$$

The corresponding free vibration frequency equation is

$$\left| \left[\begin{array}{cc} \mathbf{K}^r & \mathbf{K}^i \\ \mathbf{K}^i & \mathbf{K}^r \end{array} \right] - \omega^2 \left[\begin{array}{cc} \mathbf{M}^r & \mathbf{M}^i \\ \mathbf{M}^i & \mathbf{M}^r \end{array} \right] \right| = 0 \quad (18)$$

Let the matrices

$$\overline{\overline{\mathbf{K}}} = \left[\begin{array}{cc} \mathbf{K}^r & \mathbf{K}^i \\ \mathbf{K}^i & \mathbf{K}^r \end{array} \right] \quad (19)$$

$$\overline{\overline{\mathbf{M}}} = \left[\begin{array}{cc} \mathbf{M}^r & \mathbf{M}^i \\ \mathbf{M}^i & \mathbf{M}^r \end{array} \right] \quad (20)$$

Eq.(18) becomes

$$\left| \overline{\overline{\mathbf{K}}} - \omega^2 \overline{\overline{\mathbf{M}}} \right| = 0 \quad (21)$$

Eq. (21) represents a symmetric eigenvalue problem relating k and ω for the discretised structure, whose solutions give WFEM estimates of the dispersion relations for the continuous structure. Corresponding to each value of k in Eq.(21), there will be a discrete set of frequencies that occur in equal pairs. Each frequency will have associated with correspondence an eigenvector. This eigenvector defines the wave motion in the periodic section at that frequency.

3 Numerical investigation

As shown in Fig.1, we investigate PCs composed of copper (segment A) and epoxy (segment B) arranged in a lattice with a filling fraction $a_1:a_2=1:1$ and the lattice constant $a=150 \text{ mm}$. Table 1 shows the material parameters of copper and epoxy.

Table 1: Materials properties

Materials	Density(ρ)(Kg/m^3)	Young's modules(E) $10^{10}Pa$	Cross area(S) $10^{-4}(m^2)$
Copper	8950	16.46	1
Epoxy	1180	0.435	1

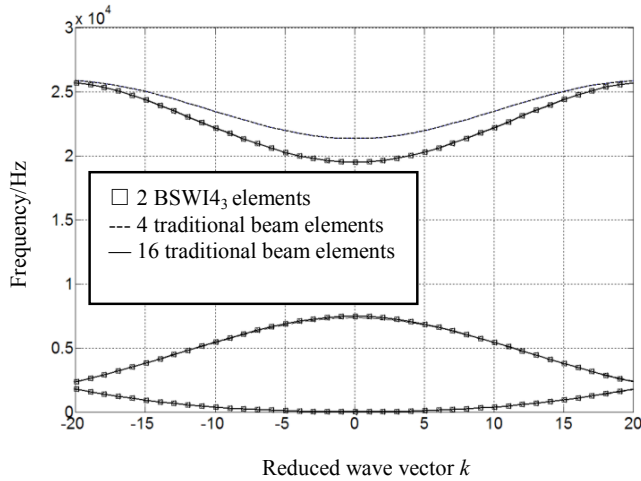


Figure 3: The band structure of WFEM (squares) and traditional FEM (dashed and solid lines)

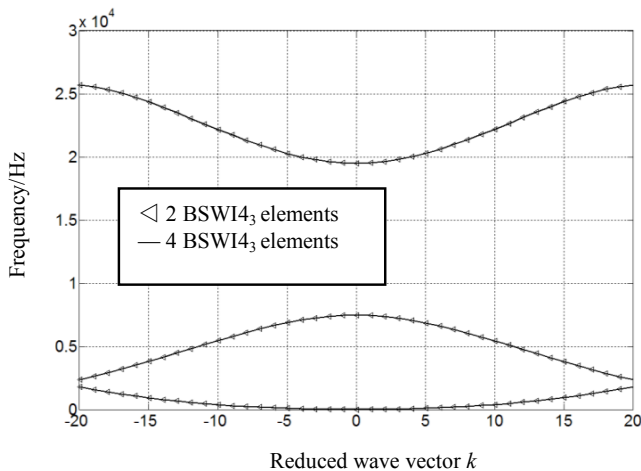


Figure 4: The band structure calculated by 2 and 4 BSWI₄₃ Euler beam elements

In order to verify the validity of the present method, we employ 2 BSWI₄₃ Euler beam elements (20 DOFs), 4 and 16 traditional Euler beam elements [Zienkiewicz et al. (2005)] (10 and 34 DOFs) to solve the band structure of the 1DPCs. The results are plotted in Fig. 3 and the squares, the dashed lines and the solid lines denote the solutions of 2 BSWI₄₃ Euler beam elements, 4 and 16 traditional Euler beam elements, respectively. From Fig.3, we find that the results from the two

methods are in good agreement and the 2 BSWI₄₃ Euler beam elements can reach the accuracy of 16 traditional beam elements. As well known, FEM is efficient and reliable to compute 1DPCs, which verifies that the developed WFEM can yield accurate results. It points out that the DOF used for traditional element more than 1.5 times of that of the present method.

The above results indicate that good calculation accuracy can be achieved for the 1DPCs by the proposed WFEM. The main advantage of the proposed method is the time savings due to the reduction of DOF.

To testify the convergence of the present wavelet FEM, we adopted 2(20 DOFs) and 4(38 DOFs) BSWI₄₃ Euler beam elements to calculate the BGs of 1DPCs, respectively. The results are shown in Fig.4. The solution of 2 elements also can reach high precision. This is because the resulting matrices are very sparse in the wavelet-based method.

Furthermore, we give a performance comparison of BSWI Euler beam element at different wavelet level, i.e., BSWI₄₃, BSWI₄₄, BSWI₄₅ and BSWI₄₆ Euler beam elements. The results are basically identical with BSWI₄₃. It illustrates BSWI₄₃ elements can gain a high accuracy to calculate the band structure.

The numerical results are presented in this paper demonstrating the accuracy, efficiency and reliability of the BSWI beam element. The fundamental cause of the good performance of BSWI beam element lies in the BSWI scaling functions with the advantages of high approximation precision and the excellent localization characteristic in space domain.

4 Conclusions

In this paper, the good approximation capability of BSWI₄_j beam element has been explored to approximate the displacement fields of 1DPCs. More specifically, two BSWI₄_j beam element are employed to discretize a unit cell and the corresponding equation of motion and further the corresponding frequency equation for calculating BGs are obtained. The numerical results show that the advantage of this method is its computational efficiency. This is reflected by the fact that it requires fewer elements, in comparison to the popular finite element method, to achieve the same solution quality. The further work is to compute BGs of 2D or 3D phononic crystals.

Acknowledgement: The authors are grateful to the support from the National Science Foundation of China (No. 51175097), the Zhejiang Provincial Natural Science Foundation for Excellent Young Scientists (No. LR13E050002) and the Project-sponsored by SRF for ROCS, SEM.

References

- Assouar, M. B.; Oudich, M.** (2011): Dispersion curves of surface acoustic waves in a two-dimensional phononic crystal. *Appl. Phys. Lett.* vol. 99, no. 12, 123505.
- Chen, X. F.; Yang, S. J.; Ma, J. X.; He, Z. J.** (2004): the construction of wavelet finite element and its application. *Finte Elem. Anal. Des*, vol. 40, no. 5, pp. 541-554.
- Chen, X. F.; Xiang, J. W.; Li, B.; He, Z. J.** (2010): A study of multiscale wavelet-based elements for adaptive finite element analysis. *Adv. Eng. Softw*, vol. 41, no. 2, pp. 196-205.
- Chen, X. F.; Yang, Z. B.; Zhang, X. W.; He, Z. J.** (2012): Modeling of wave propagation in one-dimension structures using B-spline wavelet on interval finite element. *Finite Elem. Anal. Des*, vol. 51, pp. 1-9.
- Gao, H. F.; Matsumoto, T.; Takahashi, T.; Isakari, H.** (2013a): Analysis of band structure for 2D acoustic phononic structure by BEM and the block SS method. *CMES-Comput. Model. Eng. Sci.*, vol. 90, pp. 283-301.
- Gao, H. F.; Matsumoto, T.; Takahashi, T.; Isakari H.** (2013b): Eigenvalue analysis for acoustic problem in 3D by boundary element method with the block Sakurai-Sugiura method. *Eng. Anal. Bound. Elem.*, vol. 37, pp. 914-923.
- Hang, J. G.; Ren, W. X.; Huang, Y.** (2005): A multivariable wavelet based finite element method and its application to thick plates. *Finte Elem. Anal. Des*, vol. 41, pp. 821-833.
- Hang, J. G.; Ren, W. X.; Huang, Y.** (2006): A spline wavelet finite-element method in structural mechanics. *Int. J. Num. Meth. Engng*, vol. 66, pp. 166-190.
- He, W. Y.; Ren, W. X.** (2013a): Adaptive trigonometric hermite wavelet finite element method for structural analysis. *Int. J. Struct. Stab. Dyn*, vol. 13, 1350007.
- He, W. Y.; Ren, W. X.** (2013b): Trigonometric wavelet-based method for elastic thin plate analysis. *Appl. Math. Model*, vol. 37, pp. 1607-1617.
- Kushwaha, M. S.; Halevi, P.; Dobrzynsi, L.;Diafari-Rouhani, B.** (1993): Acoustic band structure of periodic elastic composites. *Phys. Rev. Lett.* vol. 71, pp. 2022-2025.
- Kushwaha, M. S.; Halevi, P.; Martinez, G.; Dobrzynski, L.; Djafari-Rouhani, B.** (1994): Theory of acoustic band structure of periodic elastic composites. *Phys. Rev. B*, vol. 49, pp. 2313-2322.
- Ko, J.; Kurdila, A. J.; Pilant, M. S.** (1997): Triangular wavelet based finite elements via multivalued scaling equations. *Comput. Meth. Appl. Mech.Eng*, vol. 146, pp. 1-17.

- Li, B.; Dong, H. B.** (2012): Quantitative identification of multiple cracks in a rotor utilizing wavelet finite element method. *CMES-Comput. Model. Eng. Sci.*, vol. 84, no. 3, pp. 205-228.
- Li, B.; He, Z. J.** (2013): A benchmark problem for comparison of vibration-based crack identification methods. *CMES-Comput. Model. Eng. Sci.*, vol. 93, no. 4, pp. 293-316.
- Li, B.; Chen, X. F.** (2014): Wavelet-based numerical analysis: A review and classification. *Finte Elem. Anal. Des*, vol. 81, pp. 14-31.
- Moiseyenko, R. P.; Laude, V.** (2011): Material loss influence on the complex band structure and group velocity in phononic crystals. *Phys. Rev. B*, vol. 83, 064301.
- Mead, D. J.** (1973): A general theory of harmonic wave propagation in linear periodic systems with multiple coupling. *J. Sound Vib*, vol. 27, pp. 235-260.
- Tanaka, Y.; Tamura, S.-I.** (1998): Surface acoustic waves in two-dimensional periodic elastic structures. *Phys. Rev. B*, vol. 58, no. 12, pp. 7958.
- Tanaka, Y.; Tamura, S.** (1999): Acoustic stop bands of surface and bulk modes in two-dimensional phononic lattices consisting of aluminum and a polymer. *Phys. Rev. B*, vol. 60, pp. 13294-13297.
- Tarasenko, O. S.; Tarasenko, C. V.; Yurchenko, V. M.** (2004): Localization of a transverse elastic wave in a semi-bounded acoustic superlattice of ferromagnetic and superconducting layers: 1. slip boundary. *Acoust. Phys.*, vol. 50, no. 5, pp. 602-611.
- Veres, I. A.; Berer, T.** (2012): Complexity of band structures: semi-analytical finite element analysis of one-dimensional surface phononic crystals. *Phys. Rev. B*, vol. 86, 104304.
- Wilkinson, J. H.** (1965): *The Algebraic Eigenvalue Problem*. Oxford: The Clarendon Press.
- Xiang, J. W.; Chen, X. F.; He, Z. J.; Dong, H. B.** (2007): The construction of 1D wavelet finite elements for structural analysis. *Comput. Mech*, vol. 40, pp. 325-339.
- Xiang, J. W.; Chen, X. F.; He, Z. J.; Zhang, Y. H.** (2008a): A new wavelet-based thin plate element using B-spline wavelet on the interval. *Comput. Mech*, vol. 41, pp. 243-255.
- Xiang, J. W.; Chen, X. F.; Yang, L. F.; He, Z. J.** (2008b): A class of wavelet-based flat shell elements using B-spline wavelet on the interval and its applications. *CMES-Comput. Model. Eng. Sci.*, vol. 23, pp. 1-12.
- Xiang, J. W.; Liang, M.** (2011): Multiple damage detection method for beams based on multi-scale elements using Hermite cubic spline wavelet. *CMES-Comput.*

Model. Eng. Sci., vol. 73, pp. 267-298.

Xiang, J. W.; Matsumoto, T.; Wang, Y. X.; Jiang, Z. S. (2011): A hybrid of interval wavelets and wavelet finite element model for damage detection in structures. *CMES-Comput. Model. Eng. Sci.*, vol. 81, pp. 269-294.

Xiang, J. W.; Wang, Y. X.; Jiang, Z. S.; Long, J. Q.; Ma, G. (2012): Numerical simulation of plane crack using hermite cubic spline wavelet. *CMES-Comput. Model. Eng. Sci.*, vol. 88, pp. 1-16.

Yang, Z. B.; Chen, X. F.; Li, B.; He, Z. J.; Miao, H. H. (2012): Vibration analysis of curved shell using B-spline wavelet on the interval (BSWI) finite elements method and general shell theory. *CMES-Comput. Model. Eng. Sci.*, vol. 85, no. 2, pp. 129-155.

Yang, Z. B.; Chen, X. F.; Zhang, X. W.; He, Z. J. (2013): Free vibration and buckling analysis of plates using B-spline wavelet on the interval Mindlin element. *Appl. Math. Model.*, vol. 37, no. 5, pp. 3449-3466.

Yang, Z. B.; Chen, X. F.; Li, X.; Jiang, Y. Y.; Miao, H. H.; He, Z. J. (2014): Wave motion analysis in arch structures via wavelet finite element method. *J. Sound Vib.*, vol. 332, no. 2, pp. 446-469.

Yang, Z. B.; Chen, X. F.; He, Y. M.; He, Z. J.; Zhang, J. (2014): The analysis of curved beam using B-spline wavelet on interval finite element method. *Shock Vib.*, 738162.

Zienkiewicz, O. C.; Taylor, R. L.; Zhu, J. Z. (2005): *The Finite Element Method: Its Basis and Fundamentals* (Sixth edition). Oxford: Butterworth-Heinemann.